

Electrochemiluminescent Ruthenium(II) *N*-Heterocyclic Carbene Complexes: a Combined Experimental and Theoretical Study

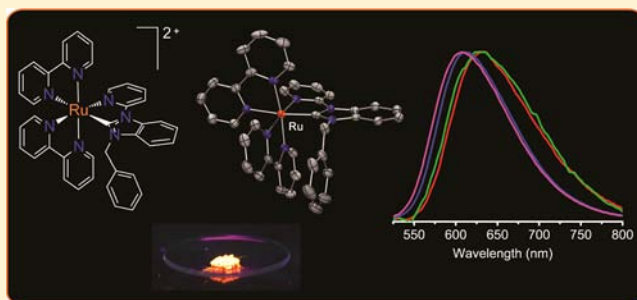
Gregory J. Barbante,^{†,‡} Paul S. Francis,[‡] Conor F. Hogan,^{*,†} Peyman R. Kheradmand,[†] David J. D. Wilson,[†] and Peter J. Barnard^{*,†}

[†]Department of Chemistry, La Trobe Institute for Molecular Science, La Trobe University, Victoria 3086, Australia

[‡]Centre for Chemistry and Biotechnology, Faculty of Science, Engineering and Built Environment, Deakin University, Geelong, Victoria 3216, Australia

S Supporting Information

ABSTRACT: A series of four Ru(II) complexes of the form $[\text{Ru}(\text{bpy})_2(\text{C}^{\wedge}\text{N})]^{2+}$ (where $\text{C}^{\wedge}\text{N}$ is a bidentate pyridine-functionalized imidazolylidene- or benzimidazolylidene-based *N*-heterocyclic carbene (NHC) ligand and bpy is 2,2'-bipyridine) have been synthesized using a Ag(I) transmetalation protocol from the Ru(II) precursor compound, $\text{Ru}(\text{bpy})_2\text{Cl}_2$. The synthesized azolium salts and Ru(II) complexes were characterized by elemental analysis, ^1H and ^{13}C NMR spectroscopy, cyclic voltammetry, and electronic absorption and emission spectroscopy. The molecular structures for two benzimidazolium salts and three Ru(II) complexes were determined by single crystal X-ray diffraction. The complexes display photoluminescence within the range 611–629 nm, with the emission wavelength of the benzimidazolylidene containing structures, slightly blue-shifted relative to the imidazolylidene containing complexes. All complexes exhibited a reversible, one-electron oxidation, which is assigned to the $\text{Ru}^{2+/3+}$ redox couple. When compared to $[\text{Ru}(\text{bpy})_3]^{2+}$, complexes of imidazolylidene containing ligands were oxidized at more negative potentials, while those of the benzimidazolylidene containing ligands were oxidized at more positive potentials. All four complexes exhibited moderately intense electrochemiluminescence (ECL) with the obtained ECL spectra closely resembling the photoluminescence spectra. The ability to predictably fine-tune the highest occupied molecular orbital (HOMO) level of the Ru(II) complexes via the flexible synthetic strategy offered by NHCs is valuable for the design of ECL-based multiplexed detection strategies.



INTRODUCTION

For several years metal complexes of *N*-heterocyclic carbene (NHC) ligands have been the subject of intense research interest for a variety of applications. Although the greatest focus has been on the development of NHC-metal complexes as homogeneous catalysts,^{1–4} there is growing interest in potential applications related to the medicinal and luminescent properties of NHC-metal complexes.^{5–8} Surprisingly, NHC complexes of relatively few metals have been evaluated for luminescence properties. Metals that have been studied include Pt(II),^{9–14} Ir(III),^{15–17} Re(I),^{18,19} and Au(I),^{20–22} while the luminescent properties of Ru(II)-NHC complexes have also occasionally been investigated.^{23–27} In an early study,²³ the photophysical properties of homoleptic Ru(II) analogues of $[\text{Ru}(\text{bpy})_3]^{2+}$ and $[\text{Ru}(\text{terpy})_2]^{2+}$ with pyridine functionalized bidentate and tridentate NHC ligands (Figure 1, i and ii) were evaluated. The $[\text{Ru}(\text{terpy})_2]^{2+}$ analogue displayed strong emission with λ_{max} of 532 nm; however, an NHC analogue of $[\text{Ru}(\text{bpy})_3]^{2+}$ was nonemissive.²³ More recently, homo- and heteroleptic²⁵ and proton-sensitive²⁶ Ru(II) complexes of pincer-type tridentate NHC ligands have been reported. Li and co-workers have synthesized Ru(II)-NHC complexes with

pyridyl substituted imidazolylidene- and benzimidazolylidene-based NHC ligands for application as sensitizers in dye-sensitized solar cells (Figure 1, iii).^{24,27} These researchers demonstrated that modification of the NHC ligand type and its substituents allowed for tuning of the electronic properties, such that the highest occupied molecular orbital (HOMO) was stabilized while the lowest unoccupied molecular orbital (LUMO) was maintained at a favorable level for charge injection into the conduction band of the TiO_2 electrode.

Apart from photoluminescence, electrochemiluminescence or electrogenerated chemiluminescence (ECL), where certain species emit light following heterogeneous electron-transfer reactions, is an area of growing importance.^{28–31} Typically, in ECL reactions the excited state is populated when an electron is transferred from a powerful reductant derived from either the reduction of the metal complex itself (annihilation ECL) or a sacrificial reagent (coreactant ECL) to the π^* orbital of a ligand of the oxidized complex. We are interested in the synthesis and development of new ECL-based sensing materials with varying

Received: February 1, 2013

Published: June 18, 2013

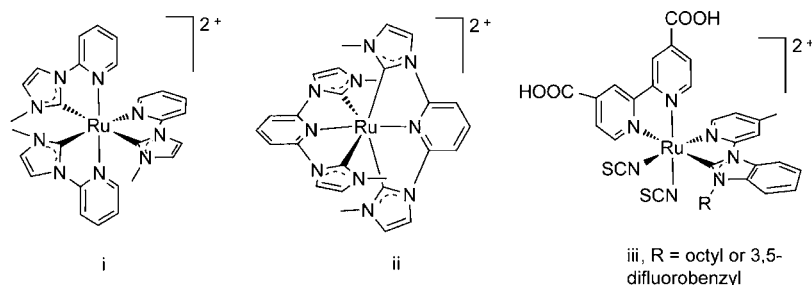


Figure 1. Structures of known Ru(II) complexes of pyridyl-functionalized NHC ligands.

emission and redox characteristics for their potential application in multiplexed sensing. Such applications require fine control over often opposing electrochemical, spectroscopic, and physical properties. As demonstrated previously,³² the electronic properties of *tris*-diimine Ru(II) complexes can be modulated by varying substituents on one of the bipyridine ligands, thus allowing the LUMO energy levels to be tuned while keeping the HOMO energy relatively constant. However, tuning of the HOMO level is also desirable, particularly for applications involving selective excitation on the basis of oxidation potential.^{33,34} While such control is readily achieved with Ir(III) complexes because the HOMO is delocalized over the metal and ligand,^{35,36} this is not true for Ru(II) complexes of diimine ligands, where the HOMO is typically metal based.

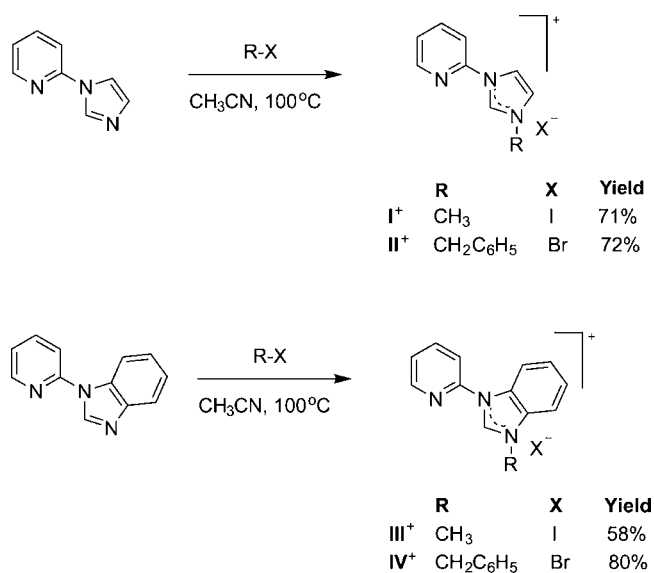
In the search for new luminescent and ECL active materials we have become interested in NHCs. Because of their excellent framework flexibility, NHC-based ligands are often more easily prepared than diimine-based systems. Additionally, the electronic properties of NHC-based ligands can be readily tuned through the choice of the azole precursor, that is, benzimidazole, imidazole, imidazoline, and triazole, as well as the wing-tip substituents.

In this paper we report the synthesis of four Ru(II) complexes incorporating two bipyridine ligands and either a pyridine-functionalized imidazolylidene or benzimidazolylidene NHC ligand via a Ag(I) transmetalation protocol. Electrochemical and spectroscopic studies show that the choice of NHC (either imidazolylidene or benzimidazolylidene) has a subtle yet distinct and predictable influence on the electron density at the metal center. The luminescence and electrochemiluminescence properties of the complexes have also been investigated. Theoretical studies provide insight into the bonding and electronic structure of these new complexes. To our knowledge, despite their prevalence in other areas of chemistry, NHCs have not previously been utilized in the development of ECL active metal complexes.

RESULTS AND DISCUSSION

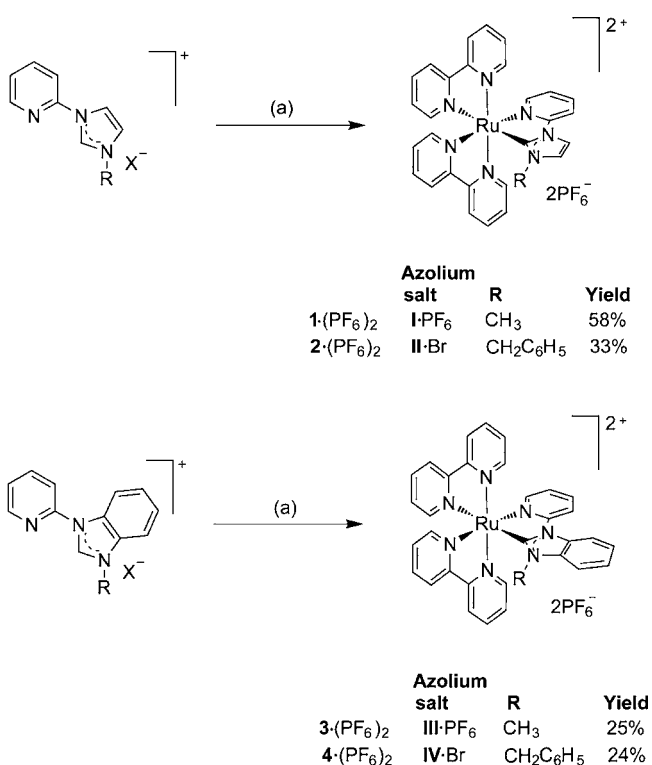
Synthesis. The azolium salt precursor, 2-pyridyl substituted azoles, 1-(2-pyridyl)imidazole and 1-(2-pyridyl)benzimidazole were prepared via an Ullmann-type Cu(I) coupling reaction between 2-bromopyridine and the chosen azole.³⁷ Formation of the desired azolium salts I-I, II-Br, III-I, and IV-Br (Scheme 1) was achieved by heating the 1-(2-pyridyl)azoles with the appropriate alkyl halide (methyl iodide or benzyl bromide) in acetonitrile. The methyl substituted azolium cations I⁺ and III⁺ have been described previously, and NHC ligands derived from them have been utilized in the synthesis of various metal-NHC complexes.^{22,23,38–41}

Scheme 1. Synthesis of Azolium Salts I-I, II-Br, III-I, and IV-Br^a



^aR-X = methyl iodide or benzyl bromide.

Formation of the desired [Ru(bpy)₂(C[^]N)]²⁺ complexes (where C[^]N is a bidentate NHC ligand derived from the azolium salts I-I, II-Br, III-I and IV-Br) was achieved using a Ag(I) transmetalation protocol and the ruthenium precursor compound, Ru(bpy)₂Cl₂ (Scheme 2). Our initial attempts to carry out this reaction at ~60 °C in solvents commonly used for NHC/Ag(I) transmetalation reactions (e.g., CH₂Cl₂ and CH₃OH)⁴² were unsuccessful, with only starting materials isolated. This is consistent with previous attempts for similar systems.⁴³ We reasoned that, although Ru(bpy)₂Cl₂ should be suitable for the Ag(I) transmetalation protocol, the lack of reactivity was most likely the result of the slow ligand substitution rates for the low-spin 4d⁶ Ru(II) complex. Therefore, in an effort to increase the reaction rate, a considerably higher reaction temperature (110 °C) was used in combination with the high boiling solvent, ethylene glycol. This approach led to the successful formation of the desired Ru(II)-NHC complexes, for both the imidazolylidene- and the benzimidazolylidene-based NHC ligands. The combination of solvent ethylene glycol with RuCl₃·XH₂O and high temperatures (140–190 °C) has been utilized previously for the formation of NHC analogues of [Ru(bpy)₃]²⁺ and [Ru(terpy)₂]²⁺ and related compounds.^{23,25,44} The Ag₂O transmetalation approach to Ru(II)-NHC complexes has also been successfully used in conjunction with the Ru(II) precursor compound [RuCl₂(cymene)]₂.^{24,43,45}

Scheme 2. Synthesis of Ruthenium(II) Complexes $1\cdot(\text{PF}_6)_2$ – $4\cdot(\text{PF}_6)_2$ ^a


^aReagents and conditions: (a) 1. azolium salt, Ag_2O in ethyleneglycol, 70°C , 4 h; 2. $\text{Ru}(\text{bpy})_2\text{Cl}_2$ 110°C , 17 h; 3. aq. KPF_6 .

The dicationic complexes were obtained as their hexafluorophosphate salts in moderate yields (24–58%) after recrystallization. In the case of the methyl functionalized azolium salts **I**⁺ and **III**⁺, it was necessary to exchange the I^- anion for PF_6^- via a metathesis reaction with potassium hexafluorophosphate prior to carrying out the Ru(II) complexation reaction. Anion exchange was required because if I^- was present in the reaction mixture, an insoluble black powder formed, and the desired compound could not be isolated.

Characterization. The structure of the azolium salts and the $[\text{Ru}(\text{bpy})_2(\text{C}^{\wedge}\text{N})]^{2+}$ complexes were confirmed by ^1H and ^{13}C NMR spectroscopy and in the case of the **III-I**, **IV-Br**, **2** $\cdot(\text{PF}_6)_2$, **3** $\cdot(\text{PF}_6)_2$, and **4** $\cdot(\text{PF}_6)_2$ by X-ray crystallography. The azolium salts gave relatively simple ^1H NMR spectra, all with a characteristic downfield resonance for the strongly deshielded pro-carbenic proton, which occurred at 10.00, 10.25, 10.44, and 10.81 ppm for **I-I**, **II-Br**, **III-I**, and **IV-Br**, respectively. For the benzyl-substituted salts **II-Br** and **IV-Br**, the methylene linker protons appear as singlets at 5.52 and 5.95 ppm, respectively. The predicted number of signals were obtained in the ^1H and ^{13}C spectra for the synthesized $[\text{Ru}(\text{bpy})_2(\text{C}^{\wedge}\text{N})]^{2+}$ complexes, consistent with the low symmetry structures (point group C_1). As expected, upon coordination of the NHC group, the signal for the azolium salt, pro-carbenic proton was absent from the ^1H NMR spectra and a characteristic downfield chemical shift was observed for the carbenic carbon atom, occurring at 192.4, 194.1, 205.8, and 207.5 ppm for the complexes **1** $\cdot(\text{PF}_6)_2$ –**4** $\cdot(\text{PF}_6)_2$ respectively. It is interesting to note the relatively large difference in the chemical shift for $\text{C}_{\text{carbene}}$ between the imidazolylidene and the benzimidazolylidene-based NHC ligands (13.4 ppm). As the metal ion, coligands and anion

are invariant for these complexes the chemical shift difference between the imidazolylidene vs benzimidazolylidene-based NHC ligands may result from greater π -back-donation for the Ru(II)-benzimidazolylidene complexes. An increase in π -back-donation of electron density from the metal to the p-orbital of the carbene carbon could be expected to result in a decrease in the π -overlap from the electron rich nitrogen atoms adjacent to the carbene and a corresponding downfield shift in the carbene resonance. For complexes **2** $\cdot(\text{PF}_6)_2$ and **4** $\cdot(\text{PF}_6)_2$, where the NHC is substituted with a benzyl group, the protons of the methylene linker are nonequivalent and an AX pattern is observed. The methylene protons are enantiotopic and the nonequivalence appears to result from the chirality associated with the octahedral *tris*(bidentate) complexes (a racemic mixture of the enantiomeric Δ and Λ forms is expected).

Selected geometric parameters for the crystal structures of **III-I**, **IV-Br**, and the Ru(II) complexes: **2** $\cdot(\text{PF}_6)_2$, **3** $\cdot(\text{PF}_6)_2$, and **4** $\cdot(\text{PF}_6)_2$ are collated in Table 1. The X-ray crystal structures of

Table 1. Selected Bond Distances (Å) and Bond Angles (deg) from X-ray Structures of Precursor Salts **III-I and **IV-Br**, and Ruthenium(II) Complexes **2** $\cdot(\text{PF}_6)_2$, **3** $\cdot(\text{PF}_6)_2$, and **4** $\cdot(\text{PF}_6)_2$**

	III-I	IV-Br	2 $\cdot(\text{PF}_6)_2$	3 $\cdot(\text{PF}_6)_2$	4 $\cdot(\text{PF}_6)_2$
C6–N2	1.340(4)	1.343(3)	1.371(5)	1.393(3)	1.394(4)
C6–N3	1.319(4)	1.317(3)	1.395(5)	1.340(3)	1.348(4)
C6–Ru1			2.004(4)	1.974(3)	1.983(3)
N1–Ru1			2.079(4)	2.070(2)	2.070(3)
N4–Ru1			2.058(4)	2.066(2)	2.067(3)
N5–Ru1			2.056(4)	2.069(2)	2.068(3)
N6–Ru1			2.112(3)	2.119(2)	2.115(3)
N7–Ru1			2.057(3)	2.061(2)	2.059(3)
N2–C6–N3	110.1(2)	110.6(2)	103.8(3)	105.3(2)	105.1(3)

the benzimidazolium salts **III-I** and **IV-Br** are illustrated in Figure 2. For compound **III-I** a short C6–H \cdots I1 distance of 2.884(2) Å, indicative of a hydrogen bond, is found between the weakly acidic proton on C6 and the iodide counterion. Similarly for **IV-Br** a hydrogen bonding interaction is observed between the proton on C6 and a bromide counterion (2.5360(2) Å), in addition to a short contact between the counterion and a benzylic proton (3.1499(3) Å).

Single crystals of the ruthenium complexes **2** $\cdot(\text{PF}_6)_2$, **3** $\cdot(\text{PF}_6)_2$, and **4** $\cdot(\text{PF}_6)_2$ were grown by slow evaporation of methanol solutions of each compound. The X-ray crystal structures of the Ru(II) cations **2**²⁺, **3**²⁺, and **4**²⁺ are shown in Figure 3. All the molecular structures display a distorted octahedral coordination geometry for the Ru(II) centers with two chelating bpy ligands and the bidentate NHC-pyridine unit. In the case of **4**²⁺, disorder was observed in the benzyl substituent on the NHC ligand. Slight differences were observed between the Ru1–C6 bond lengths for **2**²⁺ (imidazolylidene NHC) (2.004(4) Å) and **3**²⁺ and **4**²⁺ (benzimidazolylidene NHC) (1.974(3) Å and 1.983(3) Å, respectively). The Ru– $\text{C}_{\text{carbene}}$ bond distance for the imidazolylidene-based complex **2**²⁺ is similar to or shorter than those reported previously for related Ru(II) complexes (e.g., 2.014–2.116 Å,⁴⁷ 2.033(3) Å and 2.054(6) Å,⁴³ 2.004(5) Å²⁴). Comparable Ru(II) complexes with benzimidazolylidene-based ligands are rare, although for one related complex, the Ru– $\text{C}_{\text{carbene}}$ bond distance is 1.943 Å.⁴¹ A strong *trans* influence

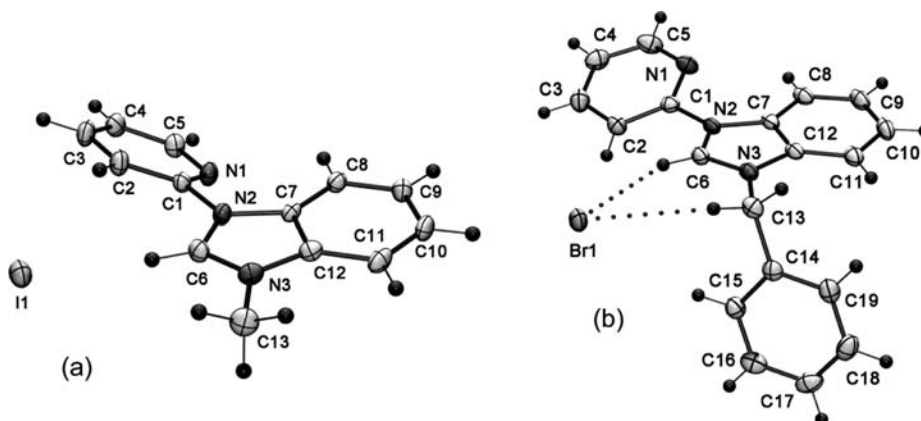


Figure 2. ORTEP⁴⁶ representations of the X-ray crystal structures of the benzimidazolium salts (a) III-I and (b) IV-Br. Thermal ellipsoids are shown at 40% probability.

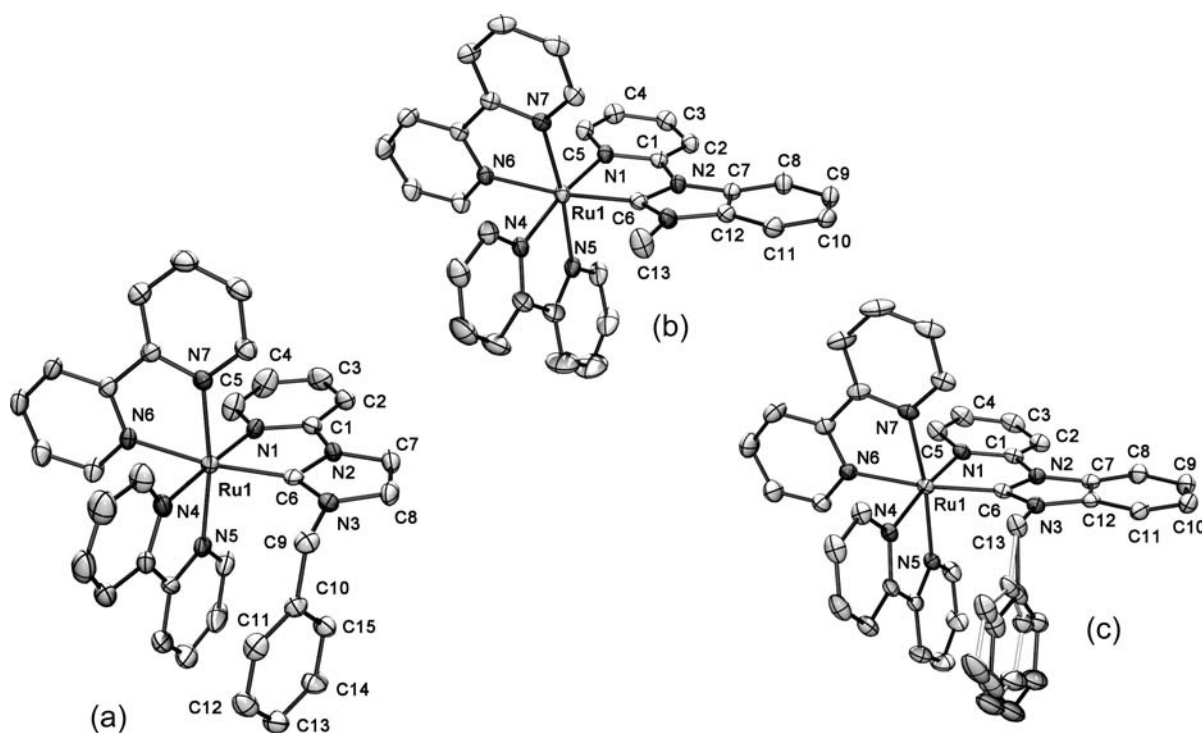


Figure 3. ORTEP⁴⁶ representations of the X-ray crystal structures of the Ru(II) cations: (a) 2^{2+} , (b) 3^{2+} , and (c) 4^{2+} . The benzyl substituent is disordered, and the site occupancy factors for the disordered atoms are 0.58 and 0.42. The hexafluorophosphate anions, hydrogen atoms, and solvents of crystallization have been omitted for clarity. Thermal ellipsoids are shown at 40% probability.

from the carbene is apparent, with a significant elongation of the Ru1–N6 bond (2.112(3), 2.119(2), and 2.115(3) Å for 2^{2+} , 3^{2+} , and 4^{2+} , respectively) when compared to the average of the other Ru1–N_{pyridyl} bond distances (2.064, 2.068, and 2.068 Å for 2^{2+} , 3^{2+} , and 4^{2+} , respectively). The *trans* influence exerted by NHCs is well-known and has been described for other Ru(II)-NHC complexes.^{24,41,43,47} Comparison of the N2–C6–N3 angle between the benzimidazolium salts (110.1(2)° and 110.6(2)° for III-I and IV-Br, respectively) and that of the Ru(II)-benzimidazolylidene complexes (105.3(2)° and 105.1(3)° for 3^{2+} and 4^{2+} , respectively) shows that upon formation and coordination of the carbene this angle becomes more acute.

Compounds $3 \cdot (\text{PF}_6)_2$ and $4 \cdot (\text{PF}_6)_2$ crystallized in the centrosymmetric space groups $C2/c$ and $P2_1/c$, respectively, indicating that the crystals are composed of a racemic mixture

of the enantiomeric Δ and Λ forms of the Ru(II) complexes. For $2 \cdot (\text{PF}_6)_2$ the structure was solved in the chiral space group $P2_1$ and the asymmetric unit contains two independent molecules, these being the Δ and Λ forms of the octahedral complex.

Absorption Spectroscopy. The UV–visible absorbance spectra for compounds $1 \cdot (\text{PF}_6)_2$ – $4 \cdot (\text{PF}_6)_2$ are similar to the expected profile for ruthenium polypyridyl complexes such as $[\text{Ru}(\text{bpy})_3]^{2+}$ (see Supporting Information, Figure S1). The visible region is dominated by broad bands of moderate intensity, which are metal to ligand charge transfer (MLCT) in nature, (i.e., $d \rightarrow \pi^*$ transitions). The UV region on the other hand is characterized by spin-allowed π – π^* ligand-centered (LC) transitions. The position of the MLCT band for each complex in acetonitrile is dependent on the identity of the auxiliary NHC ligand; for 1^{2+} and 2^{2+} it is similar to that of

$[\text{Ru}(\text{bpy})_3]^{2+}$, while for 3^{2+} and 4^{2+} (benzimidazolylidene) the MLCT band is slightly blue-shifted (see Table 2). This suggests

Table 2. Spectroscopic Properties of Ru(II) Complexes $1 \cdot (\text{PF}_6)_2$ – $4 \cdot (\text{PF}_6)_2$ ^a

	$\lambda_{\text{max}}/\text{nm}; (\epsilon/\text{M}^{-1} \text{cm}^{-1})^b$	photoluminescence $\lambda_{\text{max}}/\text{nm}^c$	ϕ_p^d
$[\text{Ru}(\text{bpy})_3] \cdot (\text{PF}_6)_2$	207, 240, 251, 285, 322, 344, 450(14800)	620	0.095
$1 \cdot (\text{PF}_6)_2$	240(30600), 256(21200,sh), 289(53400), 365(8000), 422(8900), 460(7000)	622	0.010
$2 \cdot (\text{PF}_6)_2$	240(38100), 256(2 6200,sh), 289(70300), 365(11300), 422(12200), 460(10800)	629	0.021
$3 \cdot (\text{PF}_6)_2$	248(27600), 255(26000), 291(54000), 360(7400), 408(9800), 445(7900)	611	0.007
$4 \cdot (\text{PF}_6)_2$	248(27600), 255(25000), 291(49300), 360(7400), 408(9800), 445(7100)	619	0.004

^a 1×10^{-5} M in acetonitrile. ^b λ_{max} is the position of the peak or shoulder in the absorbance or emission profile and ϵ is the molar absorptivity. ^cEmission corrected for variation in detector sensitivity with wavelength. ^dRelative quantum yield ($\text{tris}(2,2'$ -bipyridine)-ruthenium(II) = 0.095) (acetonitrile, RT, deaerated).⁴⁸

that the benzimidazolylidene NHC moiety in 3^{2+} and 4^{2+} exerts a moderate stabilizing influence on the energy of the metal based HOMO in these two complexes relative to the same MO in $[\text{Ru}(\text{bpy})_3]^{2+}$. There is also a small difference in the positions of the highest energy bands at wavelengths below 260 nm, which are shifted to slightly higher energy for 1^{2+} and 2^{2+} relative to 3^{2+} and 4^{2+} , consistent with a slight destabilization of the LUMO in the former.

Photoluminescence. The characteristic orange photoluminescence from Ru(II) diimine complexes results from the excitation of an electron from the metal-based $d(\pi_M)$ orbitals to ligand-based π^* antibonding orbitals, a metal-to-ligand charge-transfer (MLCT), followed by intersystem crossing to the lowest triplet state, from which the emission occurs. For each of the complexes 1^{2+} – 4^{2+} , intense luminescence results from the decay of this excited state. In Figure 4(a) the corrected photoluminescence spectra in deaerated CH_3CN at room temperature are shown for $1 \cdot (\text{PF}_6)_2$ – $4 \cdot (\text{PF}_6)_2$.

The emission color varies by a relatively small amount depending on the nature of the substituents. The data presented in Table 2 shows that there is a range of 18 nm (469 cm^{-1}) between the shortest and the longest wavelength-emitting complexes. The two complexes containing the imidazolylidene-based NHC ligands emit at wavelengths longer than $[\text{Ru}(\text{bpy})_3]^{2+}$, whereas the two benzimidazolylidene containing complexes emit at wavelengths shorter than the $[\text{Ru}(\text{bpy})_3]^{2+}$ standard. The values of the photoluminescent quantum yield (Φ_p) were all lower than that of $[\text{Ru}(\text{bpy})_3]^{2+}$, with 2^{2+} having the highest value at 2.1% (Table 2).

Electrochemistry. The redox properties of $1 \cdot (\text{PF}_6)_2$ – $4 \cdot (\text{PF}_6)_2$ were studied using cyclic voltammetry and the results are summarized in Table 3. Figure 5 shows the cyclic voltammetric response for $4 \cdot (\text{PF}_6)_2$ dissolved in acetonitrile. Similar electrochemical behavior is observed for complexes $1 \cdot (\text{PF}_6)_2$ – $3 \cdot (\text{PF}_6)_2$ (Supporting Information, Figure S2). Several of the voltammetric features observed are typical of those commonly displayed by ruthenium polypyridyl complexes, such as $[\text{Ru}(\text{bpy})_3]^{2+}$.⁴⁹ When scanned anodically each

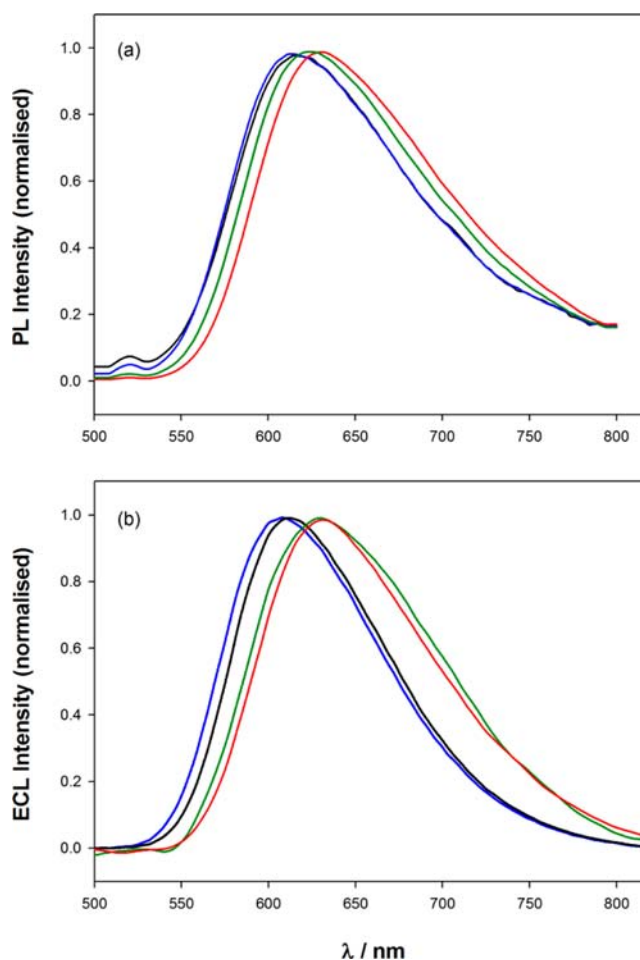


Figure 4. (a) Photoluminescence and (b) electrochemiluminescence spectra of Ru(II) complexes: $1 \cdot (\text{PF}_6)_2$ (green), $2 \cdot (\text{PF}_6)_2$ (red), $3 \cdot (\text{PF}_6)_2$ (blue), and $4 \cdot (\text{PF}_6)_2$ (black) in acetonitrile. The ECL was generated using a glassy carbon electrode in a 1 mM solution of the complex containing 0.1 M $[\text{Bu}_4\text{N}][\text{PF}_6]$ supporting electrolyte and 10 mM tripropylamine (TPA) as the coreactant.

complex exhibited a reversible, one-electron oxidation process, which can be assigned to the $\text{Ru}^{2+/3+}$ redox couple (Figure 5). The data in Table 3 indicates that the $E^{\circ'}$ values associated with the $\text{Ru}^{2+/3+}$ redox couple for complexes 1^{2+} and 2^{2+} (imidazolylidene NHC) were both substantially more negative than that for $[\text{Ru}(\text{bpy})_3]^{2+}$. In contrast, complexes 3^{2+} and 4^{2+} (benzimidazolylidene NHC) gave $E^{\circ'}$ values that were more positive than that for $[\text{Ru}(\text{bpy})_3]^{2+}$ (Table 3). The lowering of the redox potential for 1^{2+} and 2^{2+} is caused by the influence of the imidazolylidene containing ligands on the metal core, consistent with the strong σ -donating properties of the NHC relative to bipyridine as noted in a number of previous studies.^{23,25,43,50} Significantly however, this trend is not followed by the Ru(II)-benzimidazolylidene complexes which are more difficult to oxidize than $[\text{Ru}(\text{bpy})_3]^{2+}$, and suggests that the phenyl ring of the benzimidazolylidene-based NHC exerts a significant electron withdrawing influence. When examined in the context of the previously described ¹³C NMR C_{carbene} chemical shifts, the electrochemical results support the notion that the benzimidazolylidene is a stronger π -accepting ligand than imidazolylidene. That is, benzimidazolylidenes accept electron density from the metal center (π -back-bonding), thereby increasing the oxidation potential of the

Table 3. Electrochemical and Electrochemiluminescence Properties of $1\cdot(\text{PF}_6)_2$ – $4\cdot(\text{PF}_6)_2$ ^a

	Ru ^{II} /Ru ^{III} couple E°/V	bpy reductions E°/V	NHC reductions E _p /V	ΔE ^b /V	10 ⁶ D/cm ² s ⁻¹	ECL λ _{max}	rel. ECL intensity
[Ru(bpy) ₃](PF ₆) ₂	0.89	–1.75, –1.94, –2.18		2.64	5.8	620	100 ^c
1·(PF ₆) ₂	0.85	–1.78, –1.99	–2.56, –2.77	2.62	4.4	628	68
2·(PF ₆) ₂	0.84	–1.78, –1.98	–2.58, –2.79	2.63	5.83	633	95
3·(PF ₆) ₂	0.90	–1.75, –1.95	–2.56, –2.77	2.66	7.24	613	7
4·(PF ₆) ₂	0.92	–1.76, –1.96	–2.60, –2.80	2.68	5.1	608	52

^a1 mM/0.1 M (Bu₄N)PF₆ in acetonitrile. ^bElectrochemical HOMO–LUMO gap. ^cAnnihilation between [Ru(L)₃]³⁺ and [Ru(L)₃]⁺.

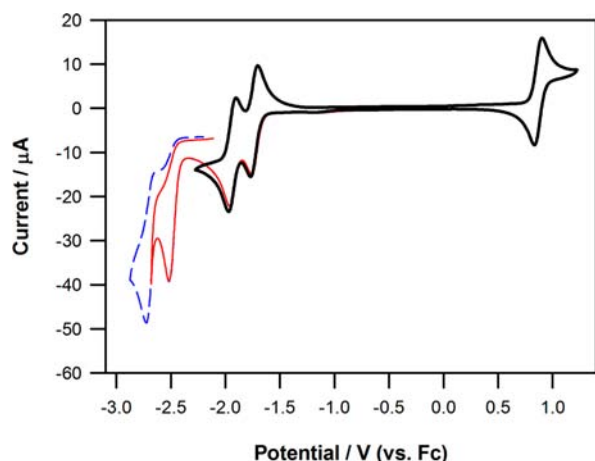


Figure 5. Cyclic voltammetric response for $4\cdot(\text{PF}_6)_2$ (1 mM) dissolved in acetonitrile containing 0.1 M [Bu₄N][PF₆]. Scan rate = 0.1 V s⁻¹, glassy carbon disk working electrode (ϕ = 3 mm). The red and blue traces show the responses when the cathodic switching potential was made sufficiently negative to encompass the third and fourth reduction processes respectively.

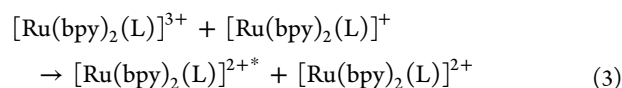
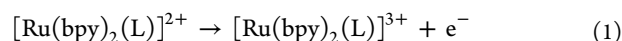
metal complex. These observations point to a destabilization of the HOMO by the NHC ligand in 1^{2+} and 2^{2+} but a net stabilization of the HOMO in 3^{2+} and 4^{2+} , which may result from a greater level of π back-bonding associated with the benzimidazolylidene NHC ligand. These combined effects result in a smaller HOMO–LUMO gap for 1^{2+} and 2^{2+} compared with 3^{2+} and 4^{2+} , consistent with the luminescence data presented in Figure 4.

When scanned cathodically, the first reductive processes for all complexes (1^{2+} – 4^{2+}) are two reversible, one-electron waves which may be confidently assigned to the stepwise reduction of the two bipyridine ligands on the basis of the theoretical calculations presented later, which indicate that the HOMOs of the bipyridine ligands are lower in energy than that of the NHC ligands. As was the case for the Ru^{2+/3+} redox couple, the potentials of the bpy reductions are influenced by the nature of the NHC ligand, albeit to a lesser degree. For 1^{2+} and 2^{2+} , the bpy-centered reduction potentials are more negative than those of [Ru(bpy)₃]²⁺, whereas the reductions associated with 3^{2+} and 4^{2+} (Table 3) do not differ significantly from this complex. These results show that the electron donating imidazolylidene ligands moderately destabilize the bipyridine based LUMO, but that the benzimidazolylidenes have little or no effect on this molecular orbital. In each case the LUMO is centered on the bpy ligand.

When scanned to more negative potentials, two irreversible reductive processes are observed which are assigned to reduction of the NHC ligand (see Figure 5, red and blue traces). On the reverse (positive-going) scan after these more negative potential excursions, a series of overlapping features

(not shown) are observed at approximately –1 V, which result from the oxidation of the products formed during the irreversible reductive processes.

Electrochemiluminescence. All four complexes exhibited intense to moderately intense electrochemiluminescence (ECL). To quantify the ability of these complexes to produce ECL, their relative annihilation ECL intensities were measured from potential step experiments where the oxidized and reduced forms were generated sequentially at the working electrode according to



Here L is the bidentate C^N imidazolylidene- or benzimidazolylidene-based NHC ligand. For all of the complexes studied, the ECL annihilation experiments resulted in emission from the electrode surface that was easily visible with the naked eye for 1 mM solutions. As shown by the data in Table 3, compounds $1\cdot(\text{PF}_6)_2$, $2\cdot(\text{PF}_6)_2$, and $4\cdot(\text{PF}_6)_2$ produced ECL intensities of a slightly lower magnitude to the benchmark ECL emitter, [Ru(bpy)₃]²⁺. As the electrochemical properties of the complexes appear uniformly favorable (in terms of reversibility and redox power), the lower ECL intensities must stem from the relatively low luminescent quantum yields (see Table 3) compared with [Ru(bpy)₃]²⁺. Normalized ECL emission spectra for $1\cdot(\text{PF}_6)_2$ – $4\cdot(\text{PF}_6)_2$ (1 mM, acetonitrile) using 10 mM TPA as the coreactant are shown in Figure 4b, and the data is summarized in Table 3. The fact that the emission profiles are essentially identical regardless of whether optical or electrochemical excitation is employed indicates that the same excited state is attained in both types of experiment.

Theoretical Studies. The mPW1PW91^{51,52}/SDD,^{53,54} TZVP⁵⁵ with acetonitrile SCRF solvent optimized geometries of the ruthenium complexes 1^{2+} – 4^{2+} (omitting PF₆⁻ counterions) are in excellent agreement with the X-ray structures (Table 1), with differences between calculated and experimental Ru–N and Ru–C bond distances all less than 0.03 Å (average deviation of 0.02 Å).

The mPW1PW91 calculated bond distances and Wiberg bond indices (WBI) for Ru–N and Ru–C reflect the difference between the imidazolylidene (1^{2+} and 2^{2+}) and benzimidazolylidene (3^{2+} and 4^{2+}) containing complexes (see Table 4). In 1^{2+} and 2^{2+} , the Ru–C6 bond distance is slightly longer than those for 3^{2+} and 4^{2+} , and this small difference is reflected in the WBI values (indicative of bond order). In contrast, there is no appreciable difference in Ru–N5 and Ru–N6 bond distances

Table 4. mPW1PW91 Calculated Bond Distances and Wiberg Bond Indices (WBI) for Complexes 1^{2+} to 4^{2+} ^a

	Ru–C6		Ru–N6		Ru–N5	
	bond (Å)	WBI	bond (Å)	WBI	bond (Å)	WBI
1^{2+}	2.018	0.72	2.152	0.31	2.086	0.44
2^{2+}	2.014	0.72	2.138	0.31	2.078	0.44
3^{2+}	1.993	0.76	2.137	0.31	2.075	0.44
4^{2+}	2.005	0.76	2.146	0.31	2.074	0.44

^amPW1PW91/SDD,TZVP optimized geometries, SCRf acetonitrile solvent. Atom labeling shown in Figure 3.

and WBI values between the imidazolylidene (1^{2+} and 2^{2+}) and benzimidazolylidene (3^{2+} and 4^{2+}) containing complexes.

The well-known *trans* influence^{24,41,43,47} from the NHC group is replicated in the theoretical results, with calculated Ru1–N6 bond distances (2.138, 2.137, and 2.146 Å for 2^{2+} , 3^{2+} , and 4^{2+} , respectively) significantly longer than the average of the other Ru1–N_{pyridyl} bond distances (2.087, 2.097, 2.082 Å for 2^{2+} , 3^{2+} , and 4^{2+} , respectively).

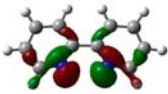
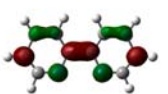
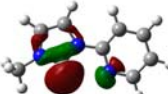
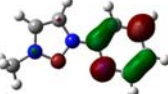
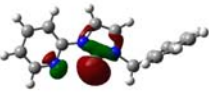
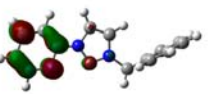

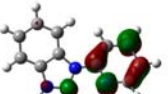
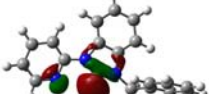

To understand the bonding and properties of the complexes, the separate ligands are discussed first.⁵⁶ Table 5 shows the HOMOs and LUMOs of the separate ligands. Note that the geometries were not optimized separately but were retained at the structure of the optimized metal–ligand complex, since optimization of free ligands led to nonplanar ligand geometries. The HOMOs of the ligands correspond to σ lone-pair orbitals on the carbon of the NHC and nitrogen of the pyridine ring.

The HOMO of the bipyridine ligand (−6.9 eV) is significantly lower lying than the carbon σ lone-pair orbitals of the imidazolylidene (−5.6 eV) and benzimidazolylidene (−5.8 eV) ligands, with the R substituent having little effect on the energies of valence orbitals. That is, the NHC σ -donor orbitals are more accessible than those of bipyridine. The relative positions of the bipyridine and NHC ligand reductions in the electrochemistry is consistent with this analysis, in that the HOMO of the bipyridine ligand is lower lying than those of the NHC ligands. The energy levels indicate that the σ -donor strength of the ligands follows the trend of imidazolylidene > benzimidazolylidene > bipyridine. It has previously been noted that NHCs have stronger σ -donating properties than bipyridine,^{23,25,43,50} which is rationalized by the analysis presented here.

Representative plots of the valence MOs of 2^{2+} are given in Figure 6. The MO plots for 1^{2+} , 3^{2+} , and 4^{2+} are provided as Supporting Information (Figures S3–S5), along with a summary of contributions from metal and ligand fragments to the HOMO and LUMO (Supporting Information, Figure S6). These confirm that the HOMO, HOMO-1, and HOMO-2 are largely metal based and, in accord with the interpretation of the electrochemical data presented in Table 3, that the LUMO and LUMO+1 are associated with the bipyridine ligands, while the LUMO+2 is associated with the NHC ligand.

Calculated energies of valence orbitals of complexes 1^{2+} – 4^{2+} and the reference compound [Ru(bpy)₃]²⁺ are presented in Table 6. The energy of the HOMOs of 3^{2+} and 4^{2+} are lower

Table 5. DFT Valence Orbitals (mPW1PW91/SDD,TZVP) of the Ligands in 1^{2+} – 4^{2+} ^a

Ligand	HOMO	LUMO
Bipyridine 2^{2+}	 −6.92	 −1.60
Imidazolylidene R = CH ₃ , 1^{2+}	 −5.62	 −0.88
Imidazolylidene R = CH ₂ Ph. 2^{2+}	 −5.59	 −0.87
Benzimidazolylidene R = CH ₃ 3^{2+}	 −5.76	 −0.92
Benzimidazolylidene R = CH ₂ Ph R 4^{2+}	 −5.81	 −0.94

^aOrbital energies are given below in eV. SCRf solvent calculation with acetonitrile solvent. Geometries of ligands are taken from 1^{2+} – 4^{2+} as listed.

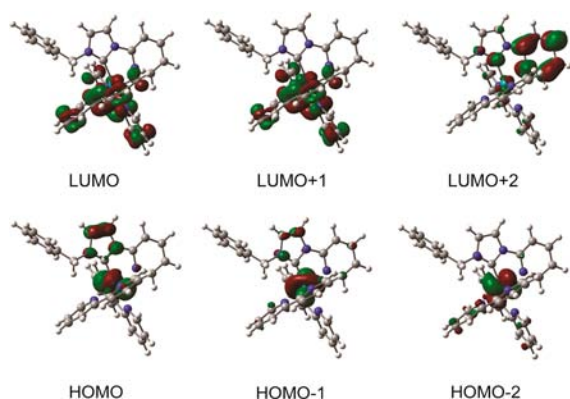


Figure 6. Valence molecular orbitals of 2^{2+} (mPW1PW91/SDD,TZVP in acetonitrile PCM-SCRF).

than those for 1^{2+} and 2^{2+} , and are in closer agreement to the energy of the HOMO of $[\text{Ru}(\text{bpy})_3]^{2+}$. It is suggested that the benzimidazolylidene exerts a greater stabilizing influence on the metal-based HOMO than does the imidazolylidene. The blue-shifted MLCT bands from the absorption spectra of 3^{2+} and 4^{2+} are consistent with the benzimidazolylidene exerting a stabilizing influence on the metal-based HOMO. The energy of the LUMO is higher for 1^{2+} and 2^{2+} compared to 3^{2+} and 4^{2+} , although the variation is much smaller than with the HOMO energies. There is a consistent trend reproduced by several density functionals in that the HOMO–LUMO energy gap of 1^{2+} – 2^{2+} is less than that of 3^{2+} – 4^{2+} (Table 6). The larger HOMO–LUMO gap for 3^{2+} and 4^{2+} (consistent with the analysis of luminescence spectra) predominantly arises from the lower HOMO energies of 3^{2+} and 4^{2+} .

For complexes 1^{2+} and 2^{2+} the destabilization of the HOMO relative to $[\text{Ru}(\text{bpy})_3]^{2+}$ dominates relative to the smaller LUMO destabilization, resulting in a net contraction of the HOMO–LUMO gap and a red shift in the luminescence for these complexes. The blue shift observed in the luminescence spectra of complexes 3^{2+} and 4^{2+} relative to $[\text{Ru}(\text{bpy})_3]^{2+}$ is primarily due to a stabilization of the HOMO. Figure S7 (Supporting Information) which compares the variance from $[\text{Ru}(\text{bpy})_3]^{2+}$ in the HOMO and LUMO energies (calculated using M06 functional) for each complex, illustrates these trends most clearly. The results of the theoretical studies are also in excellent agreement with the electrochemical data presented in Table 3 where, for example, the HOMO stabilization in 3^{2+} and 4^{2+} is manifested as a positive shift in oxidation potential.

Calculation of electronic excitations with TD-DFT (mPW1PW91) supports the above discussion of the spectroscopic and electrochemical results, with transitions in the visible region best described as MLCT, and transitions in the UV region of the spectrum dominated by intraligand charge transfer

(ILCT) transitions. For 1^{2+} and 4^{2+} an intense peak is predicted at about 271 nm, which is best described as ILCT, centered on the bpy ligands. In 3^{2+} and 4^{2+} there is an additional peak at 269 nm, which is a heavily mixed ML-IL charge transfer transition. It is suggested that this additional transition contributes to the observed differences in the absorption bands of 1^{2+} and 2^{2+} compared to 3^{2+} and 4^{2+} in this region of the spectrum. A peak at about 400 nm is associated with a MLCT transition, dominated by HOMO-2 to LUMO/LUMO+1 transitions, where the LUMO and LUMO+1 are predominantly centered on the bipyridine ligands.

Finally, an analysis of natural bonding orbitals (NBO) provides evidence of the increased π back-bonding in the benzimidazolylidene complexes. Second-order perturbation analysis of the Fock matrix indicates greater stabilization energy is obtained by donation from the Ru atom to the NHC ligand in the case of the benzimidazolylidene complexes (3^{2+} and 4^{2+}).

CONCLUSIONS

A series of $[\text{Ru}(\text{bpy})_2(\text{C}^{\wedge}\text{N})]^{2+}$ complexes (where $\text{C}^{\wedge}\text{N}$ is a pyridine-functionalized imidazolylidene- or benzimidazolylidene-based NHC ligand) were synthesized using a Ag(I) transmetalation protocol. These complexes display moderate to intense electrochemiluminescence (ECL) and represent the first examples of ECL active metal-NHC complexes reported. As the metal ion, co-ligands, and anion are invariant for this series of compounds, they represent a useful system for probing the influence of the imidazolylidene versus benzimidazolylidene NHC on the electronic properties of the complex ions. The electrochemical, spectroscopic, and theoretical studies reveal that the chosen NHC group (imidazolylidene vs benzimidazolylidene) have a subtle yet distinct and predictable influence on the electron density at the metal center. The maximum emission wavelength for both the photoluminescence and the electrochemiluminescence spectra shows a red-shift for complexes $1 \cdot (\text{PF}_6)_2$ and $2 \cdot (\text{PF}_6)_2$ relative to $[\text{Ru}(\text{bpy})_3]^{2+}$ while $3 \cdot (\text{PF}_6)_2$ and $4 \cdot (\text{PF}_6)_2$ are blue-shifted relative to this complex. In conjunction with the electrochemical findings, these data suggest that the red-shift in emission color for $1 \cdot (\text{PF}_6)_2$ and $2 \cdot (\text{PF}_6)_2$ occurs as a result of a narrowing of the HOMO–LUMO gap caused by destabilization of the HOMO. This is confirmed by the DFT calculations which show that the HOMO is significantly higher in energy for the two imidazolylidene containing complexes. The electrochemical data also suggests that the imidazolylidene NHC also has a slight destabilizing influence on the LUMO in $1 \cdot (\text{PF}_6)_2$ and $2 \cdot (\text{PF}_6)_2$, which would be expected to have the opposite effect on the emission energy. However, the DFT calculations show that this effect is small relative to the HOMO destabilization. The blue-shift in the emission maxima observed for $3 \cdot (\text{PF}_6)_2$ and $4 \cdot (\text{PF}_6)_2$ is also in accord with the electrochemical results

Table 6. DFT Calculated HOMO, LUMO, and HOMO-LUMO Energies (eV)^a

	mPW1PW91			B3LYP			M06		
	HOMO	LUMO	ΔE	HOMO	LUMO	ΔE	HOMO	LUMO	ΔE
$[\text{Ru}(\text{bpy})_3]^{2+}$	-6.50	-2.71	3.79	-6.21	-2.84	3.37	-6.29	-2.67	3.62
1^{2+}	-6.36	-2.64	3.73	-6.09	-2.77	3.32	-6.23	-2.62	3.61
2^{2+}	-6.37	-2.65	3.72	-6.09	-2.78	3.31	-6.25	-2.65	3.60
3^{2+}	-6.47	-2.67	3.80	-6.19	-2.80	3.39	-6.32	-2.65	3.67
4^{2+}	-6.49	-2.71	3.79	-6.21	-2.83	3.38	-6.36	-2.69	3.67

^aSDD,TZVP basis set and effective core potential with acetonitrile PCM SCRF.

Table 7. Crystal Refinement Data

	III-I	IV-Br	2·(PF ₆) ₂	3·(PF ₆) ₂	4·(PF ₆) ₂
empirical formula	C ₁₃ H ₁₂ N ₃ I	(C ₁₉ H ₁₆ N ₃ Br) ₂ (C ₂ H ₃ N)	C ₃₅ H ₂₉ N ₇ Ru(PF ₆) ₂	C ₃₃ H ₂₇ N ₇ ORu(PF ₆) ₂	C ₅₀ H ₃₄ N ₇ ORu(PF ₆) ₂
formula weight	337.16	773.57	938.66	928.63	1019.75
temperature/K	173	173	173	173	173
crystal system	monoclinic	monoclinic	monoclinic	monoclinic	monoclinic
space group	P ₂ ₁ /c	P ₂ ₁ /c	P ₂ ₁	C2/c	P ₂ ₁ /c
a/Å	14.7507(3)	14.0030(2)	12.5569(3)	40.444(8)	9.79520(10)
b/Å	12.1244(3)	17.7221(2)	14.8590(3)	10.140(2)	18.7887(3)
c/Å	7.18753(15)	19.8032(2)	20.3832(4)	19.104(4)	22.5522(3)
α/deg	90	90	90	90	90
β/deg	92.997(2)	133.8030(10)	104.3169(19)	113.84(3)	106.6800(10)
γ/deg	90	90	90	90	90
volume/Å ³	1283.69(5)	3546.85(7)	3685.03(12)	7166(2)	3975.84(9)
Z	4	4	4	8	4
ρ _{calc} mg/mm ³	1.745	1.449	1.692	1.721	1.704
m/mm ⁻¹	19.443	3.206	0.612	0.63	0.576
F(000)	656	1576	1880	3712	2052
crystal size/mm ³	0.07 × 0.07 × 0.02	0.1 × 0.05 × 0.05	0.18 × 0.18 × 0.18	0.18 × 0.18 × 0.08	0.15 × 0.07 × 0.05
wavelength/Å	Cu-Kα 1.54184	Cu-Kα 1.54184	Mo-Kα 0.71073	Mo-Kα 0.71073	Mo-Kα 0.71073
θ range collected	6 to 147.64°	7.94 to 140.12°	5.86 to 52.04°	6.22 to 52.04°	5.32 to 54.2°
index ranges	-18 ≤ h ≤ 18 -14 ≤ k ≤ 14 -6 ≤ l ≤ 8	-15 ≤ h ≤ 17 -12 ≤ k ≤ 21 -24 ≤ l ≤ 21	-13 ≤ h ≤ 15 -18 ≤ k ≤ 18 -24 ≤ l ≤ 25	-49 ≤ h ≤ 49 -12 ≤ k ≤ 12 -23 ≤ l ≤ 23	-12 ≤ h ≤ 12 -23 ≤ k ≤ 24 -28 ≤ l ≤ 28
reflections collected	4795	14158	22847	47151	43041
independent reflections	2513 [R(int) = 0.0229]	6701 [R(int) = 0.0201]	12928 [R(int) = 0.0203]	7064 [R(int) = 0.0224]	8736 [R(int) = 0.0264]
data/restraints/parameters	2513/0/155	6701/0/443	12928/1/1027	7064/0/516	8736/20/564
goodness-of-fit on F ₂	1.033	1.036	1.023	1.061	1.033
final R indexes [I > 2σ(I)]	R ₁ = 0.0292 wR ₂ = 0.0757	R ₁ = 0.0324 wR ₂ = 0.0889	R ₁ = 0.0321 wR ₂ = 0.0730	R ₁ = 0.0345 wR ₂ = 0.0876	R ₁ = 0.0478 wR ₂ = 0.1292
final R indexes [all data]	R ₁ = 0.0308 wR ₂ = 0.0770	R ₁ = 0.0355 wR ₂ = 0.0917	R ₁ = 0.0377 wR ₂ = 0.0767	R ₁ = 0.0382 wR ₂ = 0.0909	R ₁ = 0.0557 wR ₂ = 0.1362
largest diff. peak/hole/e Å ⁻³	0.827/-0.611	0.912/-0.828	0.540/-0.339	1.207/-0.765	1.363/-0.941

which show that the HOMO is stabilized when compared to [Ru(bpy)₃]²⁺. The influence of the benzimidazolylidene-based NHC ligand on the properties of 3·(PF₆)₂ and 4·(PF₆)₂ can be rationalized as being an effect related to π back-bonding, where back-donation of electron density from the metal to the ligand, mitigates the strong sigma donating properties commonly found for NHCs. The complexes exhibit moderately intense photoluminescence and compare well with [Ru(bpy)₃]²⁺ in terms of their electrochemiluminescence intensity. The ability to predictably fine-tune the HOMO levels using this flexible synthetic strategy is valuable for the design of ECL-based multiplexed detection strategies. Given the framework flexibility displayed by NHCs, and the decreased influence that the wingtip substituent (methyl and benzyl) have on the redox and luminescent properties of the complexes, we believe that luminescent Ru(II)-NHC complexes offer significant scope for the development of luminescent probes for biological imaging applications and for sensor development.

EXPERIMENTAL SECTION

General Procedures. All reagents were purchased from Sigma-Aldrich or Alfa Aesar and were of analytical grade or higher and were used without further purification unless otherwise stated. Dry CH₃CN and tetrahydrofuran (THF) were distilled from CaH₂ and sodium benzophenone ketyl under nitrogen, respectively. NMR spectra were recorded using a Bruker ARX-300 (300.14 MHz for ¹H, 75.48 MHz for ¹³C) NMR spectrometer and were referenced to solvent resonances. Microanalyses were performed by the Microanalytical Laboratory at the ANU Research School of Chemistry, Canberra,

Australia. All compounds were prepared in air unless otherwise specified. Mass spectra were obtained using a Bruker Esquire6000 mass spectrometer fitted with an Agilent electrospray (ESI) ion source. UV-visible spectra were recorded using a Varian Cary 50 Bio UV-visible spectrophotometer using quartz cuvettes (1 cm). Fluorescence spectra were recorded on a Varian Cary Eclipse spectrofluorimeter (5 nm band-pass, 1 nm data interval, PMT voltage: 600 V) using quartz cuvettes (1 cm).

Photoluminescence quantum yields (Φ) were determined from

$$\Phi_x = \Phi_{\text{ref}} \left(\frac{\text{Grad}_x}{\text{Grad}_{\text{ref}}} \right) \left(\frac{\eta_x^2}{\eta_{\text{ref}}^2} \right) \quad (5)$$

where ref denotes the reference complex [Ru(bpy)₃][PF₆]₂ (0.095 in CH₃CN)⁴⁸ and x denotes a sample complex, Φ is the quantum yield, Grad is the gradient of the absorbance vs integrated emission intensity graph (at least five different concentrations were used with absorbance below 0.1 and achieving η² close to 1), and η is the refractive index of the solvent. Quantum yield determinations were conducted at room temperature (21 ± 3 °C). All solutions were thoroughly degassed with nitrogen in septum sealed quartz cells prior to measurements.

Electrochemistry. Electrochemical experiments were performed using an AUTOLAB type II electrochemical station potentiostat (MEP Instruments, North Ryde, NSW, Australia) with General Purpose Electrochemical Systems (GPES) software (version 4.9). For electrochemical characterization a conventional three-electrode configuration, consisting of a 3 mm diameter glassy carbon working electrode shrouded in Teflon (CH Instruments, Austin, TX, U.S.A.), a 1 cm² platinum gauze auxiliary electrode and a silver wire quasi reference electrode. The Ru(II) complexes were prepared at a concentration of 1 mM in freshly distilled acetonitrile, with 0.1 M [Bu₄N][PF₆] as the

supporting electrolyte. Prior to each experiment, the working electrode was polished using 0.3 μm and then 0.05 μm alumina with water on a felt pad, rinsed with Milli-Q water followed by a final rinse with freshly distilled acetonitrile and dried with a stream of argon. Scan rates ranging from 0.01 to 0.5 V s^{-1} were used in cyclic voltammetry to evaluate diffusion coefficients (D) using the Randles Sevcik equation. Potentials were referenced to the ferrocene/ferrocenium couple measured in situ (1 mM) in each case.

Electrochemiluminescence (ECL). Relative ECL efficiencies (Φ_{ECL}) were evaluated, using a 3 mm diameter glassy carbon electrode, by comparison of the ECL spectra with that of the standard (1 mM $[\text{Ru}(\text{bpy})_3]^{2+}$ and 0.1 M $[\text{Bu}_4\text{N}][\text{PF}_6]$ in acetonitrile) = 100%. Annihilation ECL was generated using chronoamperometry where the cathodic and anodic potentials were stepped for 1.0 s and underwent 10 cycles. An overpotential of 0.1 V was used to generate the 3+ and 1+ forms of the Ru(II) complexes in the annihilation reactions. Co-reactant ECL were generated using a 3 mm diameter glassy carbon electrode in a 1 mM solution of the complex containing 0.1 M $[\text{Bu}_4\text{N}][\text{PF}_6]$ supporting electrolyte and 10 mM tripropylamine (TPA) as the coreactant. ECL spectra were obtained using an Ocean Optics CCD, model QE6500, UV/vis fiber optic (length 1.00 m) with a HR 4000 Breakout box trigger in conjunction with a PGstat 12 AUTOLAB potentiostat. The electrochemical cell was encased in a custom-built light-tight faraday cage.

X-ray Crystallography. Single crystals of benzimidazolium salts III-I and IV-Br were grown by slow evaporation of acetonitrile solutions of each compound. Single crystals of the ruthenium complexes 2-(PF_6)₂, 3-(PF_6)₂, and 4-(PF_6)₂ suitable for X-ray diffraction studies were grown by slow evaporation of methanol solutions of each compound. Crystallographic refinement data for all structures determined are given in Table 7. For all samples, crystals were removed from the crystallization vial and immediately coated with paratone oil on a glass slide. A suitable crystal was mounted in paratone oil on a glass fiber and cooled rapidly to 173 K in a stream of cold N_2 using an Oxford low temperature device. Diffraction data were measured using an Oxford Gemini diffractometer mounted with Mo- $\text{K}\alpha$ $\lambda = 0.71073$ Å and Cu- $\text{K}\alpha$ $\lambda = 1.54184$. Data were reduced and corrected for absorption using the Crysalis Pro program.⁵⁷ The SHELXL97 program⁵⁸ was used to solve the structures with Direct Methods, with refinement by the Full-Matrix Least-Squares refinement techniques on F^2 . The non-hydrogen atoms were refined anisotropically and hydrogen atoms were placed geometrically and refined using the riding model. Coordinates and anisotropic thermal parameters of all non-hydrogen atoms were refined. All calculations were carried out using the program Olex2.⁵⁹ Images were generated by using ORTEP-3.⁴⁶ Further XRD details are provided in the Supporting Information. CCDC 922496–922500 contains the supplementary crystallographic data for this paper. These data can be obtained free of charge from The Cambridge Crystallographic Data Centre via www.ccdc.cam.ac.uk/data_request/cif

Theoretical Calculations. Density functional theory (DFT) calculations were carried out within the Gaussian 09 suite of programs.⁶⁰ Ground state geometries were optimized in the absence of solvent with B3LYP^{61–63} and mPW1PW91^{51,52} functionals in conjunction with the 6-31+G(d) basis set^{64–66} for nonmetal atoms and the LANL2DZ basis set and core potential for ruthenium.^{53,67} Only mPW1PW91 geometry results are presented since it has been shown previously that this functional yields reliable results.^{32,68} Single-point energy calculations were carried out at the 6-31+G(d)/LANL2DZ optimized geometries using the SDD basis and core potential (MWB)^{53,54} for ruthenium and the TZVP basis set⁵⁵ for all other atoms. The polarizable continuum model (PCM)⁶⁹ self-consistent reaction field (SCRF) was used to model solvent effects at the gas-phase optimized geometries with a solvent of acetonitrile, consistent with the experimental system. Frontier MO energies were calculated using DFT MOs with mPW91PW91, B3LYP, BP86 and M06. Excitation energies to singlet and triplet excited states were investigated with TD-DFT⁷⁰ with 40 states calculated. An SCF convergence criteria of 10^{-8} a.u. was employed throughout. Molecular

orbital analysis was carried out with the AOMix program⁷¹ and NBO 5.9.⁷²

Synthesis. 1-(2-Pyridyl)imidazole. This compound was prepared using a modified literature procedure.³⁷ A mixture of imidazole (3.4 g, 50 mmol), 2-bromopyridine (4.9 mL, 50 mmol), potassium *tert*-butoxide (7.8 g, 70 mmol), CuI (0.48 g, 2.5 mmol), benzotriazole (0.6 g, 5 mmol), and DMSO (50 mL) was heated at 110 °C for 14 h under N_2 . Water (50 mL) was added, and the mixture was extracted with ethyl acetate (3 \times 100 mL). The organic extracts were washed with brine (100 mL), dried with Na_2SO_4 , and the solvent removed under reduced pressure. After purification on silica, with ethyl acetate/hexane (3:1 v/v) as the eluent, the product was obtained as a pale orange crystalline solid (Yield: 4.1 g, 60%). ¹H NMR (d_6 -DMSO): $\delta = 8.49$ (s, 1H), 8.45–8.47 (m, 1H), 7.92–7.99 (m, 2H), 7.76 (d, $J = 7.5$ Hz, 1H), 7.31 (dd, $J = 4.4, 3.9$ Hz, 1H), 7.09 (s, 1H). ¹³C NMR (d_6 -DMSO): $\delta = 148.9, 148.7, 139.8, 135.0, 130.1, 122.4, 116.6, 112.8$.

1-(2-Pyridyl)benzimidazole. This compound was prepared as described for 1-(2-pyridyl)imidazole, from 2-bromopyridine (9.8 mL, 100 mmol), benzimidazole (11.8 g, 100 mmol), potassium *tert*-butoxide (15.6 g, 140 mmol), CuI (0.96 g, 5 mmol) and benzotriazole (1.2 g, 10 mmol) and DMSO (100 mL). After purification on silica, with ethyl acetate/hexane (1:1, v/v) as the eluent, the product was obtained as a brown oil (Yield: 7.6 g, 39%). ¹H NMR (d_6 -DMSO): $\delta = 8.90$ (s, 1H), 8.59–8.62 (m, 1H), 8.26 (d, $J = 7.2$ Hz, 1H), 8.01–8.04 (m, 1H), 7.90 (d, $J = 8.4$ Hz, 1H), 7.72–7.75 (m, 1H), 7.29–7.43 (m, 3H). ¹³C NMR (d_6 -DMSO): $\delta = 150.0, 149.1, 144.5, 142.2, 139.7, 132.0, 124.0, 123.1, 122.1, 119.9, 114.7, 113.9$.

I-I. A mixture of 1-(2-pyridyl)imidazole (1 g, 6.9 mmol) and CH_3I (1 g, 7 mmol) in CH_3CN (80 mL) was refluxed for 19 h under N_2 . The solvent was removed under reduced pressure, and the crude product recrystallized from CH_3CN and ether. The product was obtained as a white crystalline solid (Yield: 1.41 g, 71%). ¹H NMR (d_6 -DMSO): $\delta = 10.00$ (s, 1H), 8.62 (m, 1H), 8.46 (dd, $J = 2.1, 1.8$ Hz, 1H), 8.19 (dd, $J = 6.3, 5.7$ Hz, 1H), 7.93–7.99 (m, 2H), 7.59 (dd, $J = 4.2, 2.1$ Hz, 1H), 3.94 (s, 3H). ¹³C NMR (d_6 -DMSO): $\delta = 149.3, 146.4, 140.7, 135.6, 125.3, 124.9, 119.1, 114.2, 36.5$. ESI-MS: $m/z = 160.1$ (I^+) calcd. For $\text{C}_9\text{H}_{10}\text{N}_3 = 160.09$.

I-PF₆. Aqueous solutions of I-I (0.2 g, 7 mmol) and KPF_6 (0.15 g, 8 mmol) were mixed and left to stand for 0.5 h. The white crystalline precipitate of I-PF₆ was collected by vacuum filtration (Yield: 0.2 g, 93%). ¹H NMR (d_6 -DMSO): $\delta = 10.00$ (s, 1H), 8.60–8.62 (m, 1H), 8.45 (dd, $J = 2.1, 1.8$ Hz, 1H), 8.18 (dd, $J = 6.3, 5.7$ Hz, 1H), 7.92–7.97 (m, 2H), 7.61 (dd, $J = 4.2, 2.1$ Hz, 1H), 3.94 (s, 3H). ESI-MS: $m/z = 160.1$ (I^+) calcd. For $\text{C}_9\text{H}_{10}\text{N}_3 = 160.09$.

II-Br. This compound was prepared as described for I-I, from 1-(2-pyridyl)imidazole (1.0 g, 7 mmol) and benzylbromide (0.8 mL, 7 mmol). The crude product was obtained as a brown oil and was purified by trituration with acetone (Yield: 1.66 g, 72%). ¹H NMR (d_6 -DMSO): $\delta = 10.25$ (s, 1H), 8.61–8.63 (m, 1H), 8.51 (dd, $J = 2.1, 1.8$ Hz, 1H), 8.18 (dd, $J = 6.3, 6$ Hz, 1H), 8.02 (d, $J = 6$ Hz, 2H), 7.61 (dd, $J = 4.8, 4.2$ Hz, 1H), 7.47–7.51 (m, 2H), 7.36–7.44 (m, 3H), 5.52 (s, 2H, CH_2). ¹³C NMR (d_6 -DMSO): $\delta = 149.3, 146.5, 140.6, 135.2, 134.5, 129.1, 128.9, 128.6, 125.3, 123.6, 119.9, 114.4, 52.6$. Found: C, 53.83; H, 4.62; N, 12.57%. $\text{C}_{15}\text{H}_{14}\text{N}_3\text{Br}\cdot\text{H}_2\text{O}$ requires C, 53.91; H, 4.83; N, 12.57%. ESI-MS: $m/z = 236.1$ (II^+) calcd. For $\text{C}_{15}\text{H}_{14}\text{N}_3 = 236.12$.

III-I. This compound was prepared as described for I-I, from 1-(2-pyridyl)benzimidazole (1.5 g, 7.7 mmol) and CH_3I (1.1 g, 7.7 mmol). The product was obtained as a white crystalline solid (Yield: 1.5 g, 58%). ¹H NMR (d_6 -DMSO): $\delta = 10.44$ (s, 1H), 8.74–8.76 (m, 1H), 8.41–8.45 (m, 1H), 8.25 (dd, $J = 6.3, 5.7$ Hz, 1H), 8.08–8.12 (m, 1H), 8.01 (d, $J = 8.1$ Hz, 1H), 7.66–7.79 (m, 3H), 4.17 (s, 3H). ¹³C NMR (d_6 -DMSO): $\delta = 149.6, 147.4, 142.8, 140.7, 132.4, 129.4, 127.8, 127.2, 125.1, 116.9, 115.8, 114.0, 33.9$. ESI-MS: $m/z = 210.1$ (III^+) calcd. For $\text{C}_{13}\text{H}_{12}\text{N}_3 = 210.10$.

III-PF₆. This compound was prepared as described for I-PF₆ from III-I (0.2 g, 0.6 mmol) and KPF_6 (0.13 g, 0.7 mmol) (Yield: 0.2 g, 94%). ¹H NMR (d_6 -DMSO): $\delta = 10.42$ (s, 1H), 8.74–8.76 (m, 1H), 8.42–8.45 (m, 1H), 8.23 (dd, $J = 6.3, 5.7$ Hz, 1H), 8.08–8.12 (m,

1H), 7.98 (d, $J = 8.1$ Hz, 1H), 7.66–7.79 (m, 3H), 4.17 (s, 3H). ESI-MS: $m/z = 210.1$ (III^+) calcd. For $\text{C}_{13}\text{H}_{12}\text{N}_3 = 210.10$.

IV-Br. This compound was prepared as described for I-I, from 1-(2-pyridyl)benzimidazole (1 g, 5 mmol) and benzyl bromide (0.61 mL, 5 mmol). The product was obtained as a white crystalline solid (Yield: 1.47 g, 80%). ^1H NMR (d_6 -DMSO): $\delta = 10.81$ (s, 1H), 8.75–8.77 (m, 1H), 8.44–8.47 (m, 1H), 8.27 (dd, $J = 6.3, 5.7$ Hz, 1H), 8.12 (d, $J = 8.1$ Hz, 1H), 7.97 (d, $J = 4.5$ Hz, 1H), 7.64–7.74 (m, 3H), 7.61 (d, $J = 1.2$ Hz, 2H), 7.30–7.43 (m, 3H), 5.95 (s, 2H). ^{13}C NMR (d_6 -DMSO): $\delta = 149.4, 147.5, 142.8, 140.6, 133.6, 131.3, 129.8, 129.0, 128.9, 128.8, 128.6, 127.8, 127.3, 125.2, 117.2, 116.3, 114.4, 50.5$. Found: C, 62.64; H, 4.60; N, 11.67%. $\text{C}_{19}\text{H}_{16}\text{N}_3\text{Br}$ requires C, 62.31; H, 4.40; N, 11.47%. ESI-MS: $m/z = 286.1$ (IV^+) calcd. For $\text{C}_{19}\text{H}_{16}\text{N}_3 = 286.13$.

1·(PF₆)₂. A mixture of I-PF₆ (0.2 g, 0.66 mmol) and Ag₂O (0.23 g, 0.94 mmol) in ethylene glycol (10 mL) was heated in the dark at 70 °C for 4 h under N₂. Ru(bpy)₂Cl₂ (0.32 g, 0.66 mmol) was added and the temperature increased to 110 °C; this temperature was maintained for 17 h. The hot reaction mixture was filtered through Celite, and water (100 mL) and KPF₆ (0.78 g, 4.2 mmol) were added to the filtrate. After 1 h the orange precipitate was collected and recrystallized from methanol giving the product as a dark orange solid (Yield: 0.33 g, 58%). ^1H NMR (d_6 -DMSO): $\delta = 8.67$ –8.79 (m, 4H), 8.52 (d, $J = 2.1$ Hz, 1H), 8.02–8.26 (m, 6H), 7.93 (d, $J = 4.8$ Hz, 1H), 7.75 (d, $J = 5.1$ Hz, 1H), 7.61 (dd, $J = 6.6, 5.1$ Hz, 2 H), 7.38–7.56 (m, 6 H), 7.24 (dd, $J = 6.3, 6$ Hz, 1H), 2.99 (s, 3H). ^{13}C NMR (d_6 -DMSO): $\delta = 192.4, 156.5, 156.3, 155.2, 155.0, 153.8, 151.3, 151.1, 150.3, 148.9, 139.8, 138.8, 137.7, 137.5, 137.4, 128.2, 128.0, 127.7, 127.4, 126.3, 124.5, 124.3, 124.2, 123.2, 117.4, 112.4, 35.3$. Found: C, 40.50; H, 3.07; N, 11.42%. $\text{C}_{29}\text{H}_{25}\text{F}_{12}\text{N}_7\text{P}_2\text{Ru}$ requires C, 40.38; H, 2.92; N, 11.37%. ESI-MS: $m/z = 718.1$ ($[\text{I} \cdot \text{PF}_6]^+$) calcd. For $\text{C}_{29}\text{H}_{25}\text{F}_6\text{N}_7\text{PRu} = 718.09$.

2·(PF₆)₂. This compound was prepared as described for I·(PF₆)₂ from II-Br (0.218 g, 0.69 mmol), Ag₂O (0.22 g, 0.94 mmol) and Ru(bpy)₂Cl₂ (0.24 g, 0.49 mmol). The product was obtained as an orange solid after recrystallization from a mixture of methanol and water. (Yield: 0.28 g, 33%). ^1H NMR (d_6 -DMSO): $\delta = 8.70$ –8.75 (m, 3H), 8.35 (d, $J = 8.4$ Hz, 1H), 8.06–8.20 (m, 6H), 8.05 (d, $J = 5.7$ Hz, 1H), 8.01 (t, $J = 7.2$ Hz, 1H), 7.82 (t, $J = 7.5$ Hz, 1H), 7.72 (d, $J = 2.4$ Hz, 1H), 7.63 (d, $J = 5.1$ Hz, 1H), 7.44–7.54 (m, 4H), 7.37 (d, $J = 4.8$ Hz, 1H), 7.32 (t, $J = 6.3$ Hz, 1H), 7.25 (t, $J = 6.3$ Hz, 1H), 7.05 (t, $J = 7.5$ Hz, 1H), 6.83 (t, $J = 7.8$ Hz, 2H), 6.03 (d, $J = 7.2$ Hz, 2H), 5.10 (d, $J = 16.8$ Hz, 1H), 4.57 (d, $J = 16.8$ Hz, 1H). ^{13}C NMR (d_6 -DMSO): $\delta = 194.1, 156.4, 156.2, 155.9, 155.2, 154.9, 153.9, 151.0, 150.5, 150.4, 148.5, 139.8, 138.8, 137.8, 137.2, 137.0, 136.9, 128.3, 128.2, 128.0, 127.3, 127.2, 127.1, 126.1, 124.5, 124.3, 124.2, 123.9, 123.7, 123.3, 118.3, 112.7, 51.8$. Found: C, 44.95; H, 3.04; N, 10.40%. $\text{C}_{35}\text{H}_{29}\text{F}_{12}\text{N}_7\text{P}_2\text{Ru}$ requires C, 44.79; H, 3.11; N, 10.45%. ESI-MS: $m/z = 794.1$ ($[\text{2} \cdot \text{PF}_6]^+$) calcd. For $\text{C}_{35}\text{H}_{29}\text{F}_6\text{N}_7\text{PRu} = 794.12$.

3·(PF₆)₂. This compound was prepared as described for I·(PF₆)₂ from III-PF₆ (0.2 g, 0.56 mmol), Ag₂O (0.19 g, 0.84 mmol), and Ru(bpy)₂Cl₂ (0.24 g, 0.5 mmol). The product was obtained as a bright orange solid after recrystallization from ethanol (Yield: 0.13 g, 25%). ^1H NMR (d_6 -DMSO): $\delta = 8.82$ (d, $J = 8.1$ Hz, 1H), 8.75 (t, $J = 7.5$ Hz, 3H), 8.65 (d, $J = 8.7$ Hz, 1H), 8.43–8.47 (m, 1H), 8.22 (dd, $J = 7.8, 6.6$ Hz, 2H), 8.06–8.18 (m, 4H), 7.76 (d, $J = 5.1$ Hz, 1H), 7.42–7.69 (m, 9H), 7.38 (t, $J = 6$ Hz, 1H), 7.28 (t, $J = 6.6$ Hz, 1H), 3.21 (s, 3H). ^{13}C NMR (d_6 -DMSO): $\delta = 205.8, 156.3, 156.2, 155.6, 154.5, 154.4, 151.5, 151.1, 150.6, 148.5, 140.1, 139.2, 138.0, 137.8, 136.9, 131.1, 128.3, 128.1, 127.9, 127.7, 124.6, 124.4, 124.2, 122.8, 113.4, 112.1, 111.1, 32.2$. Found: C, 43.46; H, 3.09; N, 10.82%. $\text{C}_{33}\text{H}_{27}\text{F}_{12}\text{N}_7\text{P}_2\text{Ru}$ requires C, 43.43; H, 2.98; N, 10.74%. ESI-MS: $m/z = 768.1$ ($[\text{3} \cdot \text{PF}_6]^+$) calcd. For $\text{C}_{33}\text{H}_{27}\text{F}_6\text{N}_7\text{PRu} = 768.10$.

4·(PF₆)₂. This compound was prepared as described for I·(PF₆)₂ from IV-Br (0.3 g, 0.82 mmol), Ag₂O (0.29 g, 1.22 mmol) and Ru(bpy)₂Cl₂ (0.40 g, 0.82 mmol). The product was obtained as a microcrystalline dark orange solid after recrystallization from a mixture of ethanol and methanol (Yield: 0.19 g, 24%). ^1H NMR (d_6 -DMSO): $\delta = 8.74$ (dd, $J = 8.4, 8.1$ Hz, 3H), 8.54 (d, $J = 8.1$ Hz, 1H), 8.27 (d, $J = 5.4$ Hz, 1H), 8.05–8.19 (m, 5H), 8.00 (dd, $J = 7.5, 8.1$ Hz, 1H), 7.82 (dd, $J = 7.5, 8.1$ Hz, 1H), 7.65 (d, $J = 5.1$ Hz, 1H), 7.26–7.58 (m, 11H), 7.04 (t, $J = 7.5$ Hz, 1H), 6.78 (dd, $J = 7.5, 7.8$ Hz, 2H), 6.02 (d,

$J = 7.5$ Hz, 2H), 5.52 (d, $J = 17.4$ Hz, 1H), 4.92 (d, $J = 17.7$ Hz, 1H). ^{13}C NMR (d_6 -DMSO): $\delta = 207.5, 156.1, 155.8, 154.4, 151.3, 150.7, 150.3, 148.2, 140.1, 139.2, 138.1, 137.7, 137.3, 136.5, 135.6, 131.5, 128.3, 128.1, 127.5, 127.4, 127.1, 124.8, 124.6, 124.4, 124.2, 123.7, 122.8, 113.6, 112.5, 111.0, 49.0$. Found: C, 46.93; H, 2.98; N, 9.73%. $\text{C}_{39}\text{H}_{31}\text{F}_{12}\text{N}_7\text{P}_2\text{Ru} \cdot \text{H}_2\text{O}$ requires C, 46.53; H, 3.30; N, 9.74%. ESI-MS: $m/z = 844.1$ ($[\text{4} \cdot \text{PF}_6]^+$) calcd. For $\text{C}_{39}\text{H}_{31}\text{F}_6\text{N}_7\text{PRu} = 844.13$.

■ ASSOCIATED CONTENT

Supporting Information

X-ray crystallographic data for III-I, IV-Br, 2·(PF₆)₂, 3·(PF₆)₂, and 4·(PF₆)₂ in CIF format and additional X-ray crystallographic details for 2·(PF₆)₂, 3·(PF₆)₂, and 4·(PF₆)₂. UV–visible absorption spectra and cyclic voltammetric response for I·(PF₆)₂–4·(PF₆)₂. Additional theoretical study results, including variance in HOMO and LUMO energies from those of [Ru(bpy)₃]²⁺ for complexes I·(PF₆)₂–4·(PF₆)₂ calculated using the M06 functional, frontier molecular orbitals of I²⁺, 3²⁺, 4²⁺ and fragment contributions to the HOMO and LUMO of complexes I²⁺–4²⁺. This material is available free of charge via the Internet at <http://pubs.acs.org>.

■ AUTHOR INFORMATION

Corresponding Author

*E-mail: p.barnard@latrobe.edu.au (P.J.B.), c.hogan@latrobe.edu.au (C.F.H.).

Notes

The authors declare no competing financial interest.

■ ACKNOWLEDGMENTS

We thank the Australian Research Council for ARC LIEF funding (LE100100109) for the X-ray diffractometer used in this work and for ARC Discovery grant funding (DP1094179).

■ REFERENCES

- Herrmann, W. A.; Köcher, C. *Angew. Chem., Int. Ed.* **1997**, *36*, 2162.
- Herrmann, W. A. *Angew. Chem., Int. Ed.* **2002**, *41*, 1290.
- Peris, E.; Crabtree, R. H. *Coord. Chem. Rev.* **2004**, *248*, 2239.
- Díez-González, S.; Marion, N.; Nolan, S. P. *Chem. Rev.* **2009**, *109*, 3612.
- Hindi, K. M.; Panzner, M. J.; Tessier, C. A.; Cannon, C. L.; Youngs, W. J. *Chem. Rev.* **2009**, *109*, 3859.
- Barnard, P. J.; Berners-Price, S. J. *Coord. Chem. Rev.* **2007**, *251*, 1889.
- Teyssoit, M.-L.; Jarrousse, A.-S.; Manin, M.; Chevry, A.; Roche, S.; Norre, F.; Beaudoin, C.; Morel, L.; Boyer, D.; Mahiou, R.; Gautier, A. *Dalton Trans.* **2009**, 6894.
- Mercs, L.; Albrecht, M. *Chem. Soc. Rev.* **2010**, *39*, 1903.
- Unger, Y.; Zeller, A.; Ahrens, S.; Strassner, T. *Chem. Commun.* **2008**, 3263.
- Unger, Y.; Zeller, A.; Taige, M. A.; Strassner, T. *Dalton Trans.* **2009**, 4786.
- Lee, C.-S.; Sabiah, S.; Wang, J.-C.; Hwang, W.-S.; Lin, I. J. B. *Organometallics* **2009**, *29*, 286.
- Unger, Y.; Meyer, D.; Strassner, T. *Dalton Trans.* **2010**, *39*, 4295.
- Unger, Y.; Meyer, D.; Molt, O.; Schildknecht, C.; Münster, I.; Wagenblast, G.; Strassner, T. *Angew. Chem., Int. Ed.* **2010**, *49*, 10214.
- Wai-Yin Sun, R.; Lok-Fung Chow, A.; Li, X.-H.; Yan, J. J.; Sin-Yin Chui, S.; Che, C.-M. *Chem. Sci.* **2011**, *2*, 728.
- Chang, C.-F.; Cheng, Y.-M.; Chi, Y.; Chiu, Y.-C.; Lin, C.-C.; Lee, G.-H.; Chou, P.-T.; Chen, C.-C.; Chang, C.-H.; Wu, C.-C. *Angew. Chem., Int. Ed.* **2008**, *47*, 4542.

- (16) Kessler, F.; Costa, R. D.; Di Censo, D.; Scopelliti, R.; Orti, E.; Bolink, H. J.; Meier, S.; Sarfert, W.; Gratzel, M.; Nazeeruddin, M. K.; Baranoff, E. *Dalton Trans.* **2012**, 41, 180.
- (17) Sajoto, T.; Djurovich, P. I.; Tamayo, A.; Yousufuddin, M.; Bau, R.; Thompson, M. E.; Holmes, R. J.; Forrest, S. R. *Inorg. Chem.* **2005**, 44, 7992.
- (18) Casson, L. A.; Muzzioli, S.; Raiteri, P.; Skelton, B. W.; Stagni, S.; Massi, M.; Brown, D. H. *Dalton Trans.* **2011**, 40, 11960.
- (19) Li, X.-W.; Li, H.-Y.; Wang, G.-F.; Chen, F.; Li, Y.-Z.; Chen, X.-T.; Zheng, Y.-X.; Xue, Z.-L. *Organometallics* **2012**, 31, 3829.
- (20) Barnard, P. J.; Baker, M. V.; Berners-Price, S. J.; Skelton, B. W.; White, A. H. *Dalton Trans.* **2004**, 1038.
- (21) Barnard, P. J.; Wedlock, L. E.; Baker, M. V.; Berners-Price, S. J.; Joyce, D. A.; Skelton, B. W.; Steer, J. H. *Angew. Chem., Int. Ed.* **2006**, 45, 5966.
- (22) Catalano, V. J.; Etogo, A. O. *J. Organomet. Chem.* **2005**, 690, 6041.
- (23) Son, S. U.; Park, K. H.; Lee, Y.-S.; Kim, B. Y.; Choi, C. H.; Lah, M. S.; Jang, Y. H.; Jang, D.-J.; Chung, Y. K. *Inorg. Chem.* **2004**, 43, 6896.
- (24) Chen, H.-S.; Chang, W.-C.; Su, C.; Li, T.-Y.; Hsu, N.-M.; Tingare, Y. S.; Li, C.-Y.; Shie, J.-H.; Li, W.-R. *Dalton Trans.* **2011**, 40, 6765.
- (25) Dinda, J.; Liatard, S.; Chauvin, J.; Jouvenot, D.; Loiseau, F. *Dalton Trans.* **2011**, 40, 3683.
- (26) Lee, C.-S.; Zhuang, R. R.; Wang, J.-C.; Hwang, W.-S.; Lin, I. J. B. *Organometallics* **2012**, 31, 4980.
- (27) Chang, W.-C.; Chen, H.-S.; Li, T.-Y.; Hsu, N.-M.; Tingare, Y. S.; Li, C.-Y.; Liu, Y.-C.; Su, C.; Li, W.-R. *Angew. Chem., Int. Ed.* **2010**, 49, 8161.
- (28) Forster, R. J.; Bertoncello, P.; Keyes, T. E. *Annu. Rev. Anal. Chem.* **2009**, 2, 359.
- (29) Miao, W. *Chem. Rev.* **2008**, 108, 2506.
- (30) Joshi, T.; Barbante, G. J.; Francis, P. S.; Hogan, C. F.; Bond, A. M.; Gasser, G.; Spiccia, L. *Inorg. Chem.* **2012**, 51, 3302.
- (31) Joshi, T.; Barbante, G. J.; Francis, P. S.; Hogan, C. F.; Bond, A. M.; Spiccia, L. *Inorg. Chem.* **2011**, 50, 12172.
- (32) Barbante, G. J.; Hogan, C. F.; Wilson, D. J. D.; Lewcenco, N. A.; Pfeffer, F. M.; Barnett, N. W.; Francis, P. S. *Analyst* **2011**, 136, 1329.
- (33) Doeven, E. H.; Zammit, E. M.; Barbante, G. J.; Hogan, C. F.; Barnett, N. W.; Francis, P. S. *Angew. Chem., Int. Ed.* **2012**, 124, 4430.
- (34) Doeven, E. H.; Zammit, E. M.; Barbante, G. J.; Francis, P. S.; Barnett, N. W.; Hogan, C. F. *Chem. Sci.* **2013**, 4, 977.
- (35) Kiran, R. V.; Hogan, C. F.; James, B. D.; Wilson, D. J. D. *Eur. J. Inorg. Chem.* **2011**, 4816.
- (36) Kiran, R. V.; Zammit, E. M.; Hogan, C. F.; James, B. D.; Barnett, N. W.; Francis, P. S. *Analyst* **2009**, 134, 1297.
- (37) Verma, A. K.; Singh, J.; Sankar, V. K.; Chaudhary, R.; Chandra, R. *Tetrahedron Lett.* **2007**, 48, 4207.
- (38) Gründemann, S.; Kovacevic, A.; Albrecht, M.; Faller, J. W.; Crabtree, R. H. *J. Am. Chem. Soc.* **2002**, 124, 10473.
- (39) Duan, L.; Wang, M.; Li, P.; Na, Y.; Wang, N.; Sun, L. *Dalton Trans.* **2007**, 1277.
- (40) Chianese, A. R.; Bremer, P. T.; Wong, C.; Reynes, R. J. *Organometallics* **2009**, 28, 5244.
- (41) Concepcion, J. J.; Jurss, J. W.; Norris, M. R.; Chen, Z.; Templeton, J. L.; Meyer, T. J. *Inorg. Chem.* **2010**, 49, 1277.
- (42) Garrison, J. C.; Youngs, W. J. *Chem. Rev.* **2005**, 105, 3978.
- (43) Ghattas, W.; Müller-Bunz, H.; Albrecht, M. *Organometallics* **2010**, 29, 6782.
- (44) Kaufhold, O.; Hahn, F. E.; Pape, T.; Hepp, A. J. *Organomet. Chem.* **2008**, 693, 3435.
- (45) Poyatos, M.; Mas-Marzá, E.; Sanaú, M.; Peris, E. *Inorg. Chem.* **2004**, 43, 1793.
- (46) Farrugia, L. J. *Appl. Crystallogr.* **1997**, 30, 565.
- (47) Cheng, Y.; Xu, H.-J.; Sun, J.-F.; Li, Y.-Z.; Chen, X.-T.; Xue, Z.-L. *Dalton Trans.* **2009**, 7132.
- (48) Suzuki, K.; Kobayashi, A.; Kaneko, S.; Takehira, K.; Yoshihara, T.; Ishida, H.; Shiina, Y.; Oishi, S.; Tobita, S. *Phys. Chem. Chem. Phys.* **2009**, 11, 9850.
- (49) Marcaccio, M.; Paolucci, F.; Roffia, S. In *Trends in Molecular Electrochemistry*; Pombeiro, A. J. L., Amatore, C., Eds.; Marcel Dekker: New York, 2004; p 228.
- (50) Das Adhikary, S.; Samanta, T.; Roymahapatra, G.; Loiseau, F.; Jouvenot, D.; Giri, S.; Chattaraj, P. K.; Dinda, J. *New J. Chem.* **2010**, 34, 1974.
- (51) Adamo, C.; Barone, V. *J. Chem. Phys.* **1998**, 108, 664.
- (52) Perdew, J. P. In *Electronic Structure of Solids '91*; Ziesche, P., Eschrig, H., Eds.; Akademie Verlag: Berlin, Germany, 1991; p 11.
- (53) Dunning, T. H., Jr.; Hay, P. J. In *Modern Theoretical Chemistry*; Schaefer, H. F., III, Ed.; Plenum: New York, 1976; Vol. 3, p 1.
- (54) Andrae, D.; Haeussermann, U.; Dolg, M.; Stoll, H.; Preuss, H. *Theor. Chim. Acta* **1990**, 77, 123.
- (55) Schaefer, A.; Horn, H.; Ahlrichs, R. *J. Chem. Phys.* **1992**, 97, 2571.
- (56) Tonner, R.; Heydenrych, G.; Frenking, G. *Chem.—Asian J.* **2007**, 2, 1555.
- (57) *CrysAlis Pro*, 171.35.11 ed.; Oxford Diffraction Ltd.: Abingdon, U.K., 2011.
- (58) Sheldrick, G. *Acta Crystallogr., Sect. A* **2008**, 64, 112.
- (59) Dolomanov, O. V.; Bourhis, L. J.; Gildea, R. J.; Howard, J. A. K.; Puschmann, H. *J. Appl. Crystallogr.* **2009**, 42, 339.
- (60) Frisch, M. J.; Trucks, G. W.; Schlegel, H. B.; Scuseria, G. E.; Robb, M. A.; Cheeseman, J. R.; Scalmani, G.; Barone, V.; Mennucci, B.; Petersson, G. A.; Nakatsuji, H.; Caricato, M.; Li, X.; Hratchian, H. P.; Izmaylov, A. F.; Bloino, J.; Zheng, G.; Sonnenberg, J. L.; Hada, M.; Ehara, M.; Toyota, K.; Fukuda, R.; Hasegawa, J.; Ishida, M.; Nakajima, T.; Honda, Y.; Kitao, O.; Nakai, H.; Vreven, T.; J. A. Montgomery, J.; Peralta, J. E.; Ogliaro, F.; Bearpark, M.; Heyd, J. J.; Brothers, E.; Kudin, K. N.; Staroverov, V. N.; Kobayashi, R.; Normand, J.; Raghavachari, K.; Rendell, A.; Burant, J. C.; Iyengar, S. S.; Tomasi, J.; Cossi, M.; Rega, N.; Millam, J. M.; Klene, M.; Knox, J. E.; Cross, J. B.; Bakken, V.; Adamo, C.; Jaramillo, J.; Gomperts, R.; Stratmann, R. E.; Yazyev, O.; Austin, A. J.; Cammi, R.; Pomelli, C.; Ochterski, J. W.; Martin, R. L.; Morokuma, K.; Zakrzewski, V. G.; Voth, G. A.; Salvador, P.; Dannenberg, J. J.; Dapprich, S.; Daniels, A. D.; Farkas, Ö.; Foresman, J. B.; Ortiz, J. V.; Cioslowski, J.; Fox, D. J. *Gaussian 09, Revision A.1*; Gaussian, Inc.: Wallingford, CT, 2009.
- (61) Becke, A. D. *Phys. Rev. A: Gen. Phys.* **1988**, 38, 3098.
- (62) Becke, A. D. *J. Chem. Phys.* **1993**, 98, 5648.
- (63) Lee, C.; Yang, W.; Parr, R. G. *Phys. Rev. B: Condens. Matter* **1988**, 37, 785.
- (64) Hehre, W. J.; Ditchfield, R.; Pople, J. A. *J. Chem. Phys.* **1972**, 56, 2257.
- (65) Hariharan, P. C.; Pople, J. A. *Theor. Chim. Acta* **1973**, 28, 213.
- (66) Clark, T.; Chandrasekhar, J.; Spitznagel, G. W.; Schleyer, P. v. R. *J. Comput. Chem.* **1983**, 4, 294.
- (67) Hay, P. J.; Wadt, W. R. *J. Chem. Phys.* **1985**, 82, 270.
- (68) Lin, J.; Wu, K.; Zhang, M. *J. Comput. Chem.* **2009**, 30, 2056.
- (69) Tomasi, J.; Mennucci, B.; Cammi, R. *Chem. Rev.* **2005**, 105, 2999.
- (70) Stratmann, R. E.; Scuseria, G. E.; Frisch, M. J. *J. Chem. Phys.* **1998**, 109, 8218.
- (71) Gorelsky, S. I.; *AOMix: Program for Molecular Orbital Analysis*, Version 6.46; University of Ottawa: Ottawa, Ontario, Canada, 2010; <http://www.sg-chem.net/>.
- (72) Glendening, E. D.; Badenhoop, J. K.; Reed, A. E.; Carpenter, J. E.; Bohmann, J. A.; Morales, C. M.; Weinhold, F.; *NBO 5.9*; Theoretical Chemistry Institute, University of Wisconsin: Madison, WI, 2001.